

A molded surface-micromachining and bulk etching release (MOSBE) fabrication platform on (1 1 1) Si for MOEMS

Mingching Wu and Weileun Fang

Department of Power Mechanical Engineering, National Tsing Hua University, Hsinchu, Taiwan

E-mail: fang@pme.nthu.edu.tw

Received 25 October 2005, in final form 29 November 2005

Published 5 January 2006

Online at stacks.iop.org/JMM/16/260

Abstract

This work attempts to integrate poly-Si thin film and single-crystal-silicon (SCS) structures in a monolithic process. The process integrated multi-depth DRIE (deep reactive ion etching), trench-refilled molding, a two poly-Si MUMPs process and (1 1 1) Si bulk micromachining to accomplish multi-thickness and multi-depth structures for superior micro-optical devices. In application, a SCS scanning mirror driven by self-aligned vertical comb-drive actuators was demonstrated. The stiffness of the mirror was significantly increased by thick SCS structures. The thin poly-Si film served as flexible torsional springs and electrical routings. The depth difference of the vertical comb electrodes was tuned by DRIE to increase the devices' stroke. Finally, a large moving space was available after the bulk Si etching. In summary, the present fabrication process, named (1 1 1) MOSBE (molded surface-micromachining and bulk etching release on (1 1 1) Si substrate), can further integrate with the MUMPs devices to establish a more powerful platform.

(Some figures in this article are in colour only in the electronic version)

1. Introduction

Micro-opto-electro-mechanical systems (MOEMS) are successfully demonstrated in various applications by means of the manipulation of moving mechanical devices, such as projection display [1], data storages [2] and optical communications [3]. Similar to their macro counterpart, the MOEMS usually consist of various mechanical components with different characteristics. For instance, the optical scanning mirror consists of a flexible torsional spring and a stiff mirror [4, 5]. As a second example, the scanner in [6] employs comb actuators with a linear in-plane motion to drive the mirror with an angular out-of-plane motion. Consequently, various fabrication processes have been investigated to realize and to integrate micromachined components with different mechanical characteristics [7, 8]. Although MOEMS devices have a lot of advantages over the existing systems, the fabrication of MOEMS devices is still a critical challenge. It is difficult to fabricate

complicated three-dimensional micro structures using existing planar micromachining processes. Thus, the mechanical characteristics of devices, such as the stiffness, flexibility and moving space are limited to these planar processes.

The MUMPs's surface micromachining process is regarded as the most popular micromachining fabrication platform for MOEMS. However, the moving space and the stiffness of poly-Si devices are limited to the thickness of the thin film materials. The poly-Si structures such as the mirror plate and the supporting beam may experience some unwanted deflections by the thin film residual stresses [9–11]. By means of DRIE and trench-refilled molding processes, such as HEXSIL [12], HARPSS [13] and MOSBE II [14], the stiffness of poly-Si devices can be improved. Moreover, the MOSBE II process also employs the bulk silicon etching to increase the moving space of the poly-Si devices [14]. On the other hand, the single-crystal silicon (SCS) is recognized as a superior material for micro optical devices [15]. Thus, the SOI process [16] and the (1 1 1) bulk micromachining

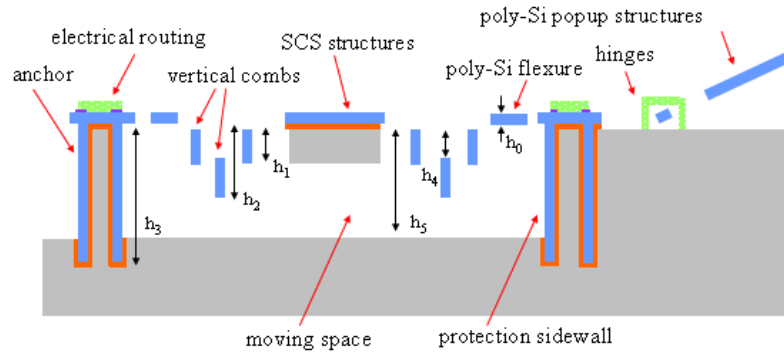


Figure 1. Schematic of (1 1 1) MOSBE process.

[17, 18] have been established to fabricate the free-standing SCS devices.

Although the MOSBE II process has enhanced the performances and varieties of poly-Si components, the stiffness and inertia are still limited to the thickness of thin film. In this regard, this work attempts to establish a novel process to further integrate the poly-Si thin film structures with the SCS thick structures. The present process, named (1 1 1) MOSBE, exploits the characteristic of fast lateral etching on (1 1 1) Si substrate to not only release the thin film components but also provide a thick SCS structure. In summary, the (1 1 1) MOSBE remains employing the thin film poly-Si as the flexible structures and electrical routing, and the trench-refilled molding components as the high aspect ratio structures and vertical comb-drive actuators. In particular, the (1 1 1) MOSBE also employs the SCS thick structure to act as the large inertia or the high stiffness components.

2. Design concept and fabrication

This study demonstrates a novel MOEMS micromachining process by integrating multi-depth DRIE etching, trench-refilled molding, a two poly-Si MUMPs process and (1 1 1) Si bulk micromachining. As illustrated in figure 1, the (1 1 1) MOSBE process attempts to accomplish multi-thickness (e.g. h_0 , h_1 and h_2-h_4) and multi-depth (e.g. substrate surface and h_4) freely suspended thin film structures and thick SCS structures (e.g. h_1 and h_3) in a monolithic process. In addition, the bulk micromachined cavity is implemented to provide a large moving space (h_5) for the device; meanwhile typical surface micromachined MUMPs structures (h_0) are also available. These poly-Si structures are also employed to act as electrical routing on SCS devices. Therefore, devices with various mechanical characteristics such as the stiff plate and the flexible spring are simultaneously accomplished through the present process.

The (1 1 1) MOSBE processes began with the deposition and patterning of thermal oxide, LPCVD (low pressure chemical vapor deposition) silicon rich nitride (Si_xN_y) and photoresist (PR), respectively. These three layers acted as etching masks for three different DRIE. As shown in figure 2(a), the PR was removed after the first DRIE. Moreover, the Si_xN_y was etched away by phosphoric acid at 180 °C after

the second DRIE. After that, the silicon oxide acted as the etching mask for the third DRIE and then was removed by hydrofluoric acid. The silicon substrate had trenches with three different depths after these three DRIEs, as indicated in figure 2(b). Moreover, the locations of trenches were all defined by the thermal oxide. The alignment of the photo masks for these three layers was not required. After a thermal oxide was grown on the substrate, these trenches were then fully refilled by the first LPCVD poly-Si film. As shown in figure 2(c), this poly-Si film was patterned to define the thin film structures. As shown in figure 2(d), a LPCVD Si_xN_y film, a PECVD SiO_2 film and a LPCVD poly-Si film were, respectively, deposited and patterned on the substrate. The LPCVD Si_xN_y and the PECVD SiO_2 films acted as the dielectric layer and the sacrificial layer, respectively. The second poly-Si film acted as the structural layer. In addition, the Si_xN_y and the second poly-Si films also served as electrical interconnections.

The fourth DRIE was exploited to trim the thickness of the poly-Si refilled inside the h_2 trenches, as indicated by h_4 in figure 2(e). Thus, the micromachined structures located at different vertical positions became available. As illustrated in figure 2(f), the Si_xN_y was deposited and patterned as the passivation layer for bulk silicon etching. Meanwhile, the poly-Si film was fully covered by the SiO_2 and the Si_xN_y films. The final photolithography process in figure 2(g) was employed to define the bulk etching windows, and followed by the patterning of SiO_2 and the Si_xN_y films by means of reactive ion etching (RIE). The fifth DRIE was used to etch the Si substrate, so as to expose the non-{1 1 1} crystal planes at the sidewalls of the trenches, as shown in figure 2(g). Moreover, the etching depth of the fifth DRIE, as indicated by h_5 in figure 2(g), was exploited to define the depth of moving space. The substrate was then immersed into KOH solution and experienced lateral silicon etching. The thermal oxide and the nitride acted as passivation layers for the poly-Si structure during bulk silicon etching. Finally, these passivation layers were removed by phosphoric acid and hydrofluoric acid. The single crystal silicon (SCS) and poly-Si structures were released from the substrate after the silicon substrate underneath was fully undercut, as shown in figure 2(h). The thickness of the SCS structures was determined by the SiO_2 protection sidewalls.

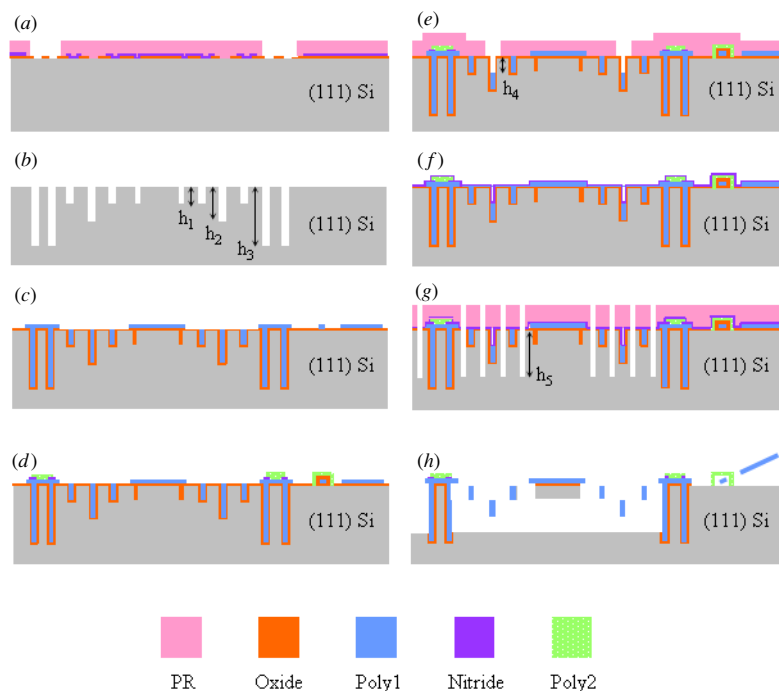


Figure 2. Detail fabrication process steps.

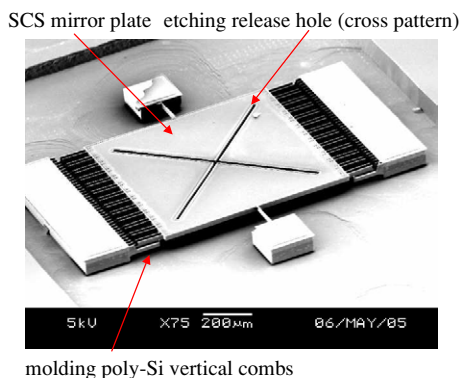


Figure 3. Fabrication result of the 1-axis scanner using the (1 1 1) MOSBE process.

3. Fabrication results and testing

Various micromachined structures have been successfully fabricated by using the (1 1 1) MOSBE process illustrated in figure 2. In this section, the fabrication and testing results of 1-axis scanning mirrors are presented to show the feasibility of this study.

3.1. Fabrication results

The 1-axis scanning mirror shown in figure 3 is a typical fabrication result realized by the (1 1 1) MOSBE process. This vertical-comb-drive scanner had a thick mirror plate and was suspended by flexible thin springs. The stationary comb electrodes and the springs were fixed to posts which anchored to the silicon substrate. The in-plane dimensions of the mirror

plate were $800\ \mu\text{m} \times 800\ \mu\text{m}$. The characteristic lengths of scanner in the out-of-plane direction ranged from $2\ \mu\text{m}$ to $80\ \mu\text{m}$. The zoom-in photo in figure 4(a) clearly shows the multi-thickness and multi-depth characteristics of structure. In the present case, the thicknesses of flexible poly-Si torsional spring and rigid SCS mirror plate were $h_0 = 2\ \mu\text{m}$ and $h_1 = 20\ \mu\text{m}$, respectively. The poly-Si thin film acting as electrical routing on SCS structures was also observed. In addition, the post which anchored to the substrate was $h_3 = 80\ \mu\text{m}$ in height. As shown in figure 4(b), the thicknesses of stationary comb electrode (h_2-h_4) and movable comb electrodes (h_1) were all $20\ \mu\text{m}$. In addition, the depth difference h_4 between stationary and movable electrodes was $20\ \mu\text{m}$ to increase the devices side instability of the vertical comb-drive actuator is substantially decreased. According to the dimensions of h_1 and h_5 , the moving space created by the lateral undercut effect of (1 1 1) Si bulk micromachining was nearly $60\ \mu\text{m}$ (h_5). This space enabled the mirror to perform large out-of-plane motion.

In short, the optical scanner realized by the present (1 1 1) MOSBE process, as demonstrated in figures 3 and 4, has the following characteristics. *First*, for the optical reflective surface of the mirror plate is rigid and large. *Second*, the thin torsional bar is flexible so as to reduce the driving voltages. *Third*, the stroke of actuator is tunable so as to improve the optical resolution. *Forth*, the scanning angle is significantly increased after the bulk silicon etching. Other optical devices are also available using the (1 1 1) MOSBE fabrication platform. For instance, figure 5(a) shows a 2-axis optical scanner. The lever mechanism driven by the vertical

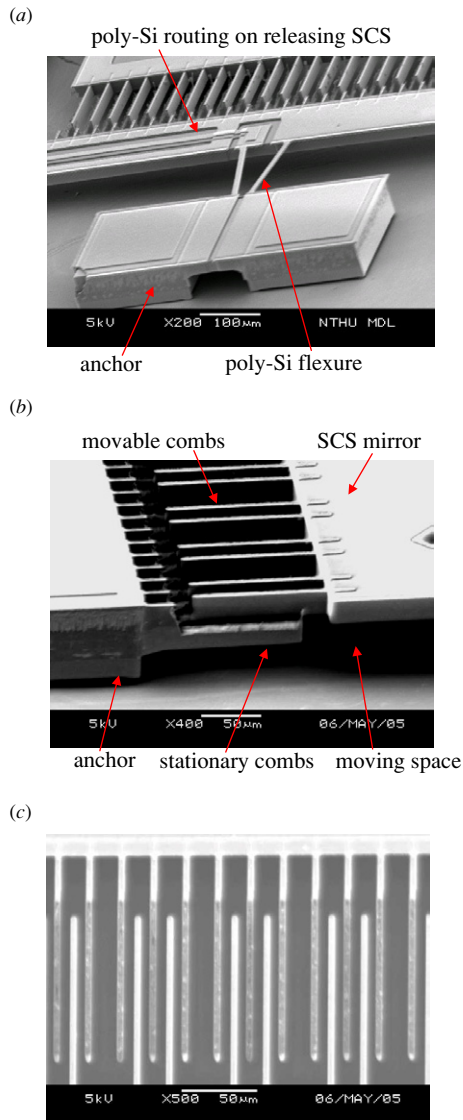


Figure 4. The zoom-in SEM photo shows the multi-thickness and multi-depth structures: (a) poly-Si as flexure and electrical routing on releasing SCS structures, (b) side view of vertical comb-drive actuators and (c) top view of comb-drive actuators.

comb actuator in figure 5(b) has the chance to act as an optical shutter.

3.2. Testing

The static and dynamic behaviors of the optical scanner in figure 3 were characterized to demonstrate the performance of the devices fabricated by the (1 1 1) MOSBE process. During the static behaviors test, a dc voltage was applied to the vertical comb actuator to drive the mirror. Meanwhile, the radius of curvature (ROC) and the angular deflection of the 20 μm thick SCS plate were characterized by a commercial optical interferometer system. Figure 6(a) shows the typical measured surface contour of the scanner. The measurement results in figure 6(b) quantitatively show the surface topology of the AB region indicated in figure 6(a). The maximum deflection of the SCS mirror plate was only 80 nm; moreover, the ROC of the

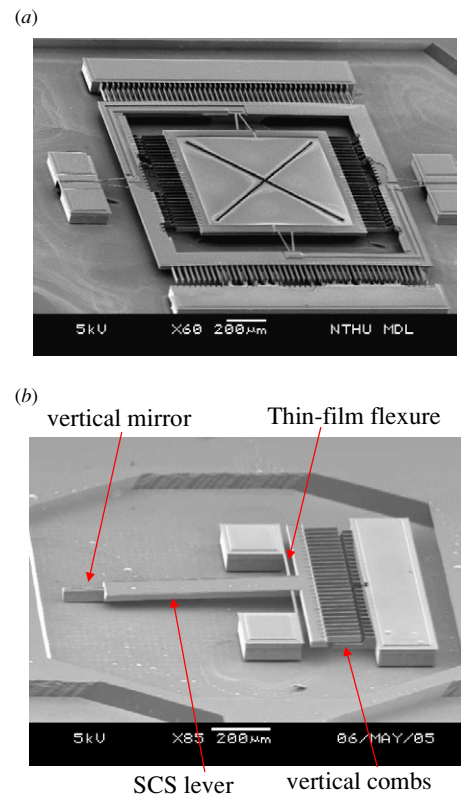


Figure 5. The micromachined devices available in the (1 1 1) MOSBE process: (a) the 2-axis optical scanner and (b) the optical shutter.

SCS mirror plate was 1.23 m. As a comparison, the typical ROC of poly-Si mirror plate was 19–100 mm [4, 9, 14]. The ROC of thick SCS mirror plate was two orders of magnitude higher than that of the poly-Si one. Thus, the SCS mirror could significantly provide a good enough reflective surface because of its stiffness. The measurement results in figure 6(c) show the surface topology of the AB region after the mirror was driven with a dc voltage. Thus, the angular deformation of the mirror was determined by the slope of this curve. In this case, the maximum displacement between torsional bar (point A) and tip (point B) of the mirror plate was 5.2 μm when the driving voltage was 35 V. Figure 7 shows the variation of the driving voltage and the angular displacement; hence, the mirror plate had a maximum scanning angle of $\pm 1.5^\circ$ at 35 V. The total optical scanning angle of the scanner was 3° .

During the dynamic behaviors test, an ac voltage was applied to the vertical comb actuator to drive the mirror. The optical laser Doppler vibrometer was used to characterize the dynamic response of the scanner. Figure 8(a) shows a typical measured frequency response. It shows that the first resonant frequency which is associated with the scanning mode (torsional vibration mode) is 3.8 kHz and the associated optical scan angle was 11.6° . The step response in figure 8(b) indicates that the settling time of optical scanning mirror is near 3 ms at atmospheric pressure. The 1D scanning images in figure 9(a) were the laser spot reflected from a 1-axis scanner driven at its first torsional mode. In addition, the concept of raster scan was employed to generate the 2D scanning images in figure 9(b) by means of two 1-axis scanners. The horizontal

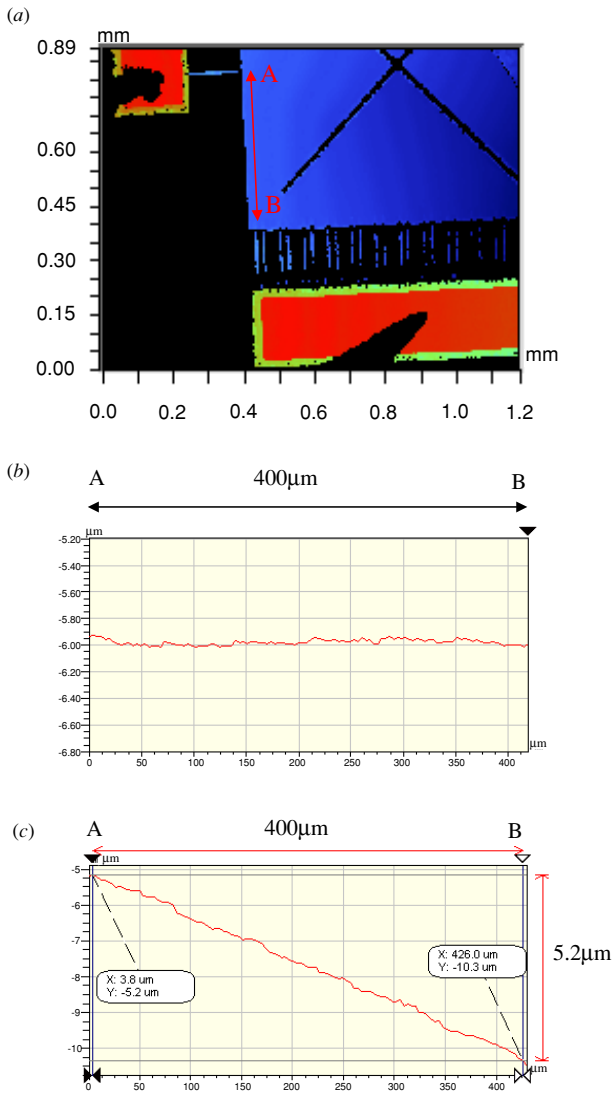


Figure 6. (a) The static results of the scanning mirror measured by the optical interferometer, (b) the ROC of the SCS mirror plate was 1.23 m and (c) the deformation profile of the mirror measured by the optical interferometer during static load-deflection test.

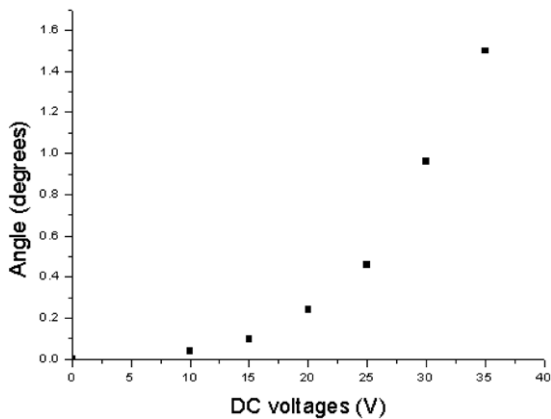


Figure 7. Variation of the driving voltage and the angular displacement of the mirror.

scanning images were reflected from the scanner driven at its first resonant frequency of 3.8 kHz; whereas the vertical

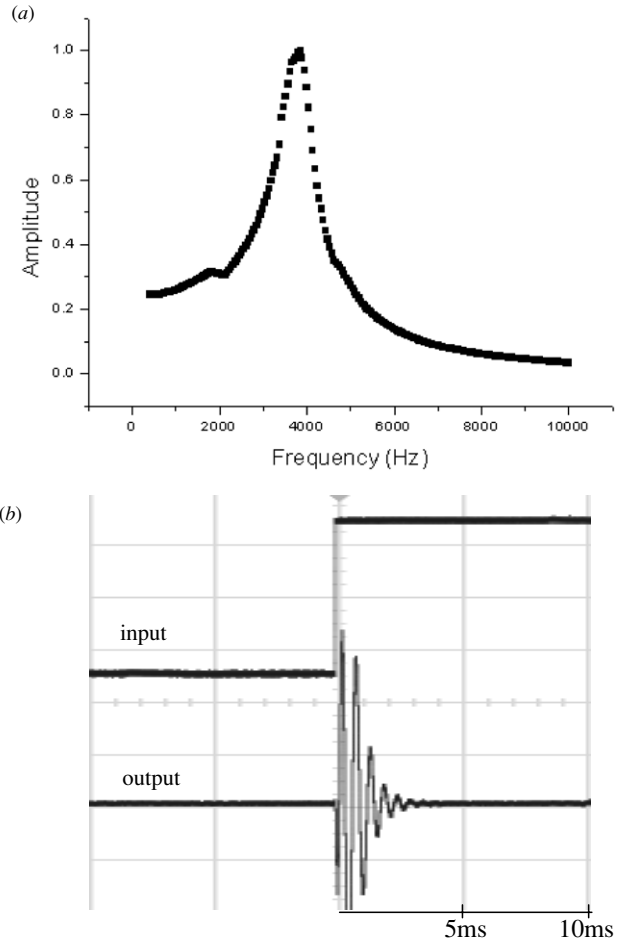


Figure 8. Experiment results for the dynamic test: (a) frequency response and (b) step response.

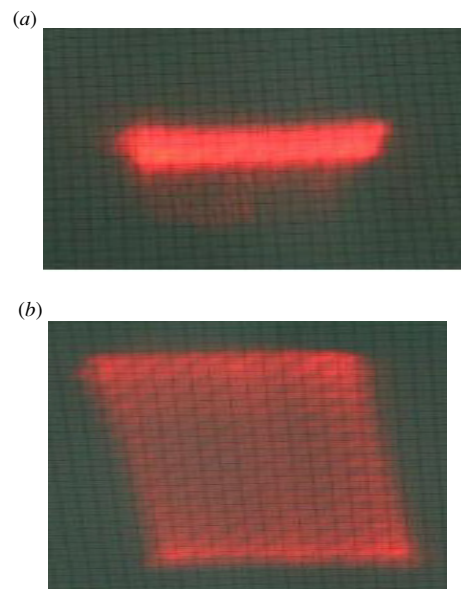


Figure 9. The trace of the reflected laser spot from the 1-axis scanner: (a) 1D scanning line, (b) 2D scanning image.

scanning images were reflected from the scanner driven at 50 Hz.

4. Conclusions and discussions

The present (1 1 1) MOSBE process has successfully integrated multi-depth DRIE etching, trench-refilled molding, the MUMPs process and (1 1 1) Si bulk micromachining to accomplish multi-thickness and multi-depth structures for superior micro-optical devices. This process offers the opportunity to fabricate thin film devices with out-of-plane characteristic lengths ranging from $\sim 1 \mu\text{m}$ to $\sim 100 \mu\text{m}$ (or even above). In application, a 1-axis scanning mirror has been fabricated and characterized. The scanner has flexible thin film springs ($2 \mu\text{m}$ thick) and rigid SCS mirror plate ($20 \mu\text{m}$ thick). The stationary and movable comb electrodes with a depth difference of $20 \mu\text{m}$ are realized to increase the devices stroke. Moreover, the moving space ($60 \mu\text{m}$) created by bulk Si etching enables the mirror to perform large out-of-plane motion. Thus, the ROC of the SCS mirror plate was reached 1.23 m and provides a reflective surface of high optical quality. As a comparison, the $2 \mu\text{m}$ thick poly-Si mirror in [4, 14] has a ROC of $<20 \text{ mm}$, and the same thickness of poly-Si rib-reinforced mirror has a ROC of 150 mm. The $22.5 \mu\text{m}$ thick SOI mirror in [4] has a ROC of 2.65 m. The scanning angle of the 1-axis mirror is $\pm 1.5^\circ$ under 35 V dc voltages and the resonant frequency is 3.8 kHz. In summary, the (1 1 1) MOSBE can further integrate with the well-known MUMPs process to establish a more powerful MOEMS platform.

Figure 9 shows that the image of the scanned laser beam is blurred. This problem is mainly led by the etching release holes on the mirror plate. In this study, the SCS structures such as mirror plate were released by means of the lateral undercut effect, and the releasing time was dependent on the planar dimensions of mirror plate. As indicated in figure 3, the etching release hole (cross pattern) was employed to reduce the bulk silicon etching time. Hence, the etching time for the $800 \mu\text{m} \times 800 \mu\text{m}$ mirror plate has been significantly reduced from 10 h to only 3 h. Thus, the tradeoff between releasing time and optical property needs to be considered while designing optical components using the present processes.

Acknowledgments

This paper was (partially) supported by the Ministry of Economic Affairs, Taiwan, under contract no. 93-EC-17-A-07-S1-0011, and by the Nation Science Council, Taiwan, under contract NSC 93-2215-E-007-005. The authors would also like to appreciate the NSC Central Regional MEMS Center (Taiwan), the Nano Facility Center of National Tsing Hua University and the NSC National Nano Device Laboratory (NDL) in providing the fabrication facilities.

References

- [1] Hornbeck L J 1996 Digital light processing: a new MEMS-based display technology *Technical Digest of the IEEE 14th Sensor Symposium (Kawasaki, Japan, June)* pp 297–304
- [2] Fan L-S, Ottesen H H, Reiley T C and Wood R W 1995 Magnetic recording-head positioning at very high track densities using a microactuator-based, two-stage servo system *IEEE Trans. Ind. Electron.* **42** 222–33
- [3] Aksyuk V A *et al* 2003 Beam-steering micromirrors for large optical cross-connects *J. Lightwave Technol.* **21** 634–42
- [4] Su G-D J, Nguyen H, Paterson P, Toshiyoshi H and Wu M C 2001 Surface-micromachined 2-D optical scanners with high-performance single-crystalline silicon micromirrors *IEEE Photonics Technol. Lett.* **13** 606–8
- [5] Milanović V 2004 Multilevel-beam SOI-MEMS fabrication and applications *J. Microelectromech. Syst.* **13** 19–30
- [6] Daneman M J, Tien N C, Solgaard O, Pisano A P, Lau K Y and Muller R S 1996 Linear microvibromotor for positioning optical components *J. Microelectromech. Syst.* **5** 159–65
- [7] Wu M C 1997 Micromachining for optical and optoelectronic systems *Proc. IEEE* **85** 1833–56
- [8] Bustillo J M, Howe R T and Muller R S 1998 Surface micromachining for microelectromechanical systems *Proc. IEEE* **86** 1552–74
- [9] Aksyuk V A, Pardo F and Bishop D J 1999 Stress-induced curvature engineering in surface-micromachined devices *Proc. SPIE* **3680** 984–93
- [10] Lin L-Y, Goldstein E L and Tkach R W 2000 On the expandability of free-space micromachined optical cross connects *J. Lightwave Technol.* **18** 482–8
- [11] Lin L Y and Goldstein E L 2002 Opportunities and challenges for MEMS in lightwave communications *J. Sel. Top. Quantum Electron.* **8** 162–72
- [12] Keller C G and Howe R T 1997 HexSil tweezers for teleoperated micro-assembly *MEMS'97, Nagoya, Japan, January* pp 72–7
- [13] Ayazi F and Najafi K 2000 High aspect-ratio combined poly and single-crystal silicon (HARPSS) MEMS technology *J. Microelectromech. Syst.* **9** 288–94
- [14] Wu M, Lai C-F and Fang W 2005 Design and fabrication of MEMS devices using the integration of MUMPs, trench-refilled molding, DRIE and bulk silicon etching processes *J. Micromech. Microeng.* **15** 535–42
- [15] Greywall D S, Busch P A, Pardo F, Carr D W, Bogart G and Soh H T 2003 Crystalline silicon tilting mirrors for optical cross-connect switches *J. Microelectromech. Syst.* **12** 708–12
- [16] Patterson P R, Hah D, Nguyen H, Toshiyoshi H, Chao R-M and Wu M C 2002 A scanning micromirror with angular comb drive actuation *IEEE MEMS'02, Las Vegas, NV, January* pp 544–7
- [17] Hu H, Lin H, Fang W and Chou B 2001 The diagnostic micromachined beams on (1 1 1) substrate *Sensors Actuators A* **93** 258–65
- [18] Hsieh J and Fang W 2002 A boron etch-stop assisted lateral silicon etching process for improved high-aspect-ratio silicon micromachining and its applications *J. Micromech. Microeng.* **12** 574–81